View metadata, citation and similar papers at core.ac.uk

brought to you by CORE

provided by Elsevier - Publisher Connector

Biochimica et Biophysica Acta 1838 (2014) 2899–2909

Contents lists available at ScienceDirect

Biochimica et Biophysica Acta

journal homepage: www.elsevier.com/locate/bbamem

Elucidation of mechanisms of interaction of a multifunctional peptide *Pa*-MAP with lipid membranes

Jéssica M. Nascimento [a], Maria D.L. Oliveira [b], Octávio L. Franco [c], Ludovico Migliolo [c], Celso P. de Melo [d], César A.S. Andrade [a,b,*]

[a] Programa de Pós-Graduação em Inovação Terapêutica, Universidade Federal de Pernambuco, 50670-901 Recife, PE, Brazil
[b] Departamento de Bioquímica, Universidade Federal de Pernambuco, 50670-901 Recife, PE, Brazil
[c] Centro de Análise Proteômicas e Bioquímicas de Brasília, Universidade Católica de Brasília, Brasília, DF, Brazil
[d] Departamento de Física, Universidade Federal de Pernambuco, 50670-901 Recife, PE, Brazil

ARTICLE INFO

Article history:
Received 3 June 2014
Received in revised form 28 July 2014
Accepted 1 August 2014
Available online 7 August 2014

Keywords:
Pleuronectes americanus
Multifunctional peptide
Antimicrobial
Membrane
Electrical impedance spectroscopy

ABSTRACT

This work aims to investigate the possible mechanism of action of the homologue peptide *Pa*-MAP based on the Antarctic fish *Pleuronectes americanus*, through a study by electrical impedance spectroscopy (EIS) of models of bilayer lipid membranes supported (BLM-s) on solid substrates. For comparison and validation of the data obtained by EIS, we also conducted a study evaluating the human peptide LL-37, whose mechanism of action is well described in the literature: its dielectric response was found to be similar to that of *Pa*-MAP. The results obtained indicate that *Pa*-MAP has a good potential for use as a membrane-disrupting peptide and also suggest that the corresponding mechanism of action occurs according to the carpet model followed by a detergent-like effect. The addition of either one of these peptides at different concentrations resulted in a drastic decrease in the membrane's resistance, after just 1 min of exposure. Additionally, it was seen that the peptides *Pa*-MAP and LL-37 may act on membranes with different charges, in an indication of a possible broad spectrum antimicrobial activity. These interactions with different membrane compositions have been attributed to the peptides' structure, mainly due to the presence of many hydrophobic amino acid residues, as observed by *in silico* studies. Here, we describe the *Pa*-MAP mechanism of action for the first time. Furthermore, we report the data demonstrating that EIS can be used for studies of peptide–membranes interaction, even when small changes on the surface of the electrode can be detected.

© 2014 Elsevier B.V. All rights reserved.

1. Introduction

The indiscriminate use of antibiotics has been an important risk factor for emergence of resistance in microorganisms and, as a result, intensive research is required for the development of novel antimicrobial agents [1]. In recent years, a large number of protein compounds – known as antimicrobial peptides (AMPs) – have been isolated from numerous sources, such as bacteria, plants, insects, amphibians and mammals [2]. In fact, since their discovery in the 1980s, AMPs have been heralded as a promising alternative to today's antibiotics [3]. Most antibiotics have specific targets, including proteins and other macromolecules; AMPs have a different mechanism of action and usually attack microbial membranes, due to their hydrophobicity. In some cases they also present a cationic amphipathic structure that allows the electrostatic attraction toward anionic lipids in the microorganisms' membranes to prevail, as an initial step, which is followed by pore formation in the membrane, leading to the cell death [4].

In spite of the fact that the discovery of new AMPs began with the identification of active peptides from natural sources, nowadays most research activity pursues the rational design of synthetic peptide analogs through structure–function studies [5]. In general, the main physical features common to the AMPs are a cationic charge, which promotes selectivity for negatively charged microbial cytoplasmic membranes over zwitterionic mammalian membranes, and a significant proportion of hydrophobic residues that facilitate interactions with the fatty acyl chains [6]. Additionally, the understanding of peptide–membrane interaction may contribute to the discovery and rational design of new biopharmaceuticals with high efficiency in controlling pathogenic microorganisms.

Another class of peptides that has been studied, but with less intensity, corresponds to the antifreezing peptides (AFPs). These proteinaceous compounds, which are found in organisms living in frozen environments, such as Arctic and Antarctic fishes, inhibit ice crystal growth in their fluids [7]. The family of type I AFPs has commonly been characterized from winter flounder (*Pleuronectes americanus*) *via*

* Corresponding author at: Departamento de Bioquímica, Universidade Federal de Pernambuco, 50670-901 Recife, PE, Brazil. Tel.: +55 81 2126x8450; fax: +55 81 2126x8576.
E-mail address: csrandrade@gmail.com (C.A.S. Andrade).

http://dx.doi.org/10.1016/j.bbamem.2014.08.002
0005-2736/© 2014 Elsevier B.V. All rights reserved.

two peptides, named HPLC-6 (4000 Da) and HPLC-8 (3300 Da), which have low molecular masses [8]. This characteristic was utilized as basis for creation of a peptide analog named *Pa*-MAP [31]. *Pa*-MAP showed deleterious activities against different targets such as cancer, bacterial and fungal cells, as well as viruses. Otherwise, *Pa*-MAP did not show any toxicity against mammalian cells [31]. Moreover, *Pa*-MAP was also evaluated *in vivo* toward bacterial infections, showing the ability to control systemic infections caused by *Escherichia coli* [9]. Its molecular mechanism of action seems to be correlated to the presence of hydrophobic residues, since the N-terminal group is charged at pH 7 [31], suggesting a lipid binding peptide. Furthermore, the theoretical *Pa*-MAP three-dimensional structure consists of an alanine-rich α-helix composed of 11 amino acids with two imperfect motif repetitions ($X_{10}T$, where X is any amino acid residue and T is threonine) [31]. A clear connection between the functional features of AMP and AFP may be observed.

In recent years, studies have been developed to understand the mode of action of peptides by analysis of peptide–membrane interactions. For this, simple models of membranes comprising different lipid compositions that mimic the original composition of bacterial membranes [5,10,11] were adopted. Among these models, lipid vesicles or liposomes, Langmuir–Blodgett layers and bilayer lipid membranes (BLM) are the most commonly used [11]. BLM supported on solid substrates (BLM-s), such as hydrophilic metals (Pt, Au, Ag, Cu, Ni, stainless steel or vitreous carbon), have dynamic properties and the required mechanical stability to allow the use of such systems as template biomembranes [12]. In addition, BLM-s have been widely used in studies of electrochemical biosensors [13] and of the behavior of ion channels [14].

Despite numerous studies on AMPs, there are still many questions to be answered about their mechanisms of action. Part of this lack of understanding occurs due to intrinsic limitations in the experimental techniques used to decipher their molecular mechanisms [15]. The most traditional technique used for the study of AMP membrane disorders consists of vesicle leakage assays, which use fluorescent probes [16] to examine the escape of polar compounds through the vesicle lipid membranes, as a result of AMP action. However, this technique suffers from several limitations, because both the ability to detect disturbances in the membrane and the small physical size of the substances to be analyzed usually require the use of higher AMP concentrations. Thus, these trials in AMP action mechanisms commonly report only the decrease in the gradient of the analyte concentration, merely stating the cumulative AMP effects on the membrane structure, and do not account for fundamental membrane–molecular peptide interactions [15].

As a way to avoid some of the previously described limitations, electrical impedance spectroscopy could be used in the investigation of membrane–AMP interactions, since it is a very sensitive technique that allows the real time monitoring of even small changes on the electrode surface coated with biological molecules [17]. Impedance spectroscopy has been used to unravel AMPs' mechanisms of action, since it is a robust technique that allows not only the study of a wide variety of AMPs, but also the analysis of other membrane-associated molecules (such as toxins, amyloid proteins and polymeric compounds), even when present in small quantities [17,18]. These characteristics provide satisfactory results in real time monitoring of the effects of active peptides on lipid membranes and allow the direct measurements of the bilayer resistance and capacitance [15,18,19]. Stainless steel has been extensively used as an inexpensive and appropriate substrate to obtain self-assembled lipid bilayers for electrical measurements [20–22]. In addition, other authors showed that by using stainless steel electrodes it is possible to obtain more stable BLM-s compared to other metals, such as silver and iridium [23].

In summary, the present work helps to decipher the possible mechanism of action of *Pa*-MAP, an analog peptide derived from the Antarctic fish *P. americanus*, by studying models of phospholipid membranes through electrical impedance spectroscopy (EIS) associated with molecular modeling, dynamics and docking studies. In this manner, important contributions to the understanding of peptide/biological membrane interactions are clearly provided. Moreover, we also focus on the types of cellular damage induced by *Pa*-MAP. All these data were further compared to those resulting from the use of the human peptide cathelicidin LL-37, which has a broad antimicrobial activity and whose action mode is already known [24,25].

2. Experimental

2.1. Materials

The phospholipid 1,2-dipalmitoyl-sn-glycero-3-phosphatidylcholine (DPPC) was obtained from Sigma Chemical (St. Louis, USA). Solid-phase cathelicidin LL-37 (sequence LLGDFFRKSKEKIGKEFKRIVQRIKDFLRNLVPRTES) with 95% purity, synthesized by the Fmoc technique, was purchased from China Peptides (Hong Kong, China). All chemicals and solvents were of analytical grade and they were used as received, without further purification. All purified water used was obtained from a Milli-Q plus (Billerica, USA) system. Amino acid derivatives and other reagents for the solid-phase peptide synthesis were from Merck-Nova Biochem (Whitehouse Station, NJ, USA), Peptides International (Louisville, KY) or Sigma-Aldrich (St. Louis, USA).

2.2. Solid-phase Pa-MAP synthesis

Pa-MAP was based on the design for two 11-residue repeating segments from HPLC-8, with the following sequence: H-HTASDAAAAAALTAANAAAAAAASMA-NH_2. The peptide was synthesized by the stepwise solid-phase method, using the N-9-fluorenylmethyloxycarbonyl (Fmoc) strategy with a Rink amide resin (0.52 mmol g^{-1}). Side chain protecting groups were t-butyl for threonine and (triphenyl)methyl for histidine. Couplings were performed with 1,3-diisopropylcarbodiimide/1-hydroxybenzotriazole (DIC/HOBt) in N,N-dimethylformamide (DMF) for 60 to 120 min. Fmoc deprotections (15 min, twice) were performed with 4-methylpiperidine: DMF solution (1:4 v/v). Cleavage from the resin and deprotection of side chains were performed with trifluoroacetic acid (TFA):water:1,2-ethanedithiol (EDT):triisopropylsilane (TIS), 94.0:2.5:2.5:1.0, by volume, at 24 °C for 90 min. After this, the crude product was precipitated with cold diisopropyl ether, collected by filtration and solubilized in 200 mL aqueous acetonitrile at 50% (by volume). The extracted peptide was twice freeze-dried for purification.

2.3. Peptide purification

Pa-MAP was solubilized in 0.1% trifluoroacetic acid (TFA) aqueous solution and filtered with a Millex filter 0.22 μm (Millipore-Merck, Billerica, MA). The crude extract was submitted to semi-preparative reverse-phase high-performance liquid chromatography (RP-HPLC), C18 NST, 5 mm, 250 mm and 610 mm, using the following mobile phase conditions: H_2O:ACN:TFA (95:05:0.1, v:v:v) for 5 min, then a linear gradient to H_2O:ACN:TFA (05:95:0.1, v:v:v) for 60 min, at a flow rate of 2.5 mL min^{-1} [26]. The experiments were conducted at room temperature and monitored at 216 nm. Fractions were manually collected and lyophilized. For all experiments reported here, the synthetic peptide concentrations were determined by using the measurement of absorbance at 205, 215 and 225 nm, as described by Murphy and Kies [27].

2.4. Mass spectrometry analyses

Pa-MAP and LL-37 molecular masses and purity degree were determined by using matrix-assisted laser desorption/ionization time of

flight mass spectrometry analysis on an UltraFlex III MALDI-ToF MS/MS (Bruker Daltonics, Billerica, USA). The purified peptide was dissolved in a minimum volume of water that was mixed with an α-cyano-4-hydroxycinnamic acid saturated matrix solution (1:3, v:v), spotted onto a MALDI target plate and dried at room temperature for 5 min. The a-cyano-4-hydroxycinnamic acid matrix solution was prepared at 50 mM in H_2O:ACN:TFA (50:50:0.3, v:v:v). Peptide monoisotopic mass was obtained in the reflector mode with external calibration, using the Peptide Calibration Standard II for mass spectrometry (up to 4000 Da mass range, Bruker Daltonics, Billerica, MA).

2.5. Modification of the electrode

The phospholipid membranes were obtained by self-assembly on a stainless steel electrode using the dip-coating method [28]. First, the stainless steel electrode was immersed in a chloroform solution of DPPC (1 mg mL^{-1}) for 10 min, to obtain the phospholipid bilayer on the electrode surface. Subsequently, the electrode containing the deposited phospholipid bilayer was transferred to a measurement cell containing deionized water, and the EIS measurements were performed at intervals of 5 min. After reaching the maximum time of deposition (30 min), the electrode containing the lipid membrane was removed from the measurement cell and immersed in other solution containing the *Pa*-MAP or LL-37 at two standard concentrations (10 and 100 μg mL^{-1}). After the waiting time in the peptide solution for each interval of 5 min, the electrode was washed and, subsequently, returned to the measurement cell. We used a separated peptide solution to avoid any interference during the measurements. Before each lipid membrane deposition, an EIS measurement on a clean (unmodified) electrode was performed in deionized water, as a reference to allow the evaluation of each subsequent modification step.

2.6. Electrical measurements

Electrical impedance measurements were performed on a SI 1260 impedance analyzer (Solartron, UK), varying the frequency of 1 Hz–1 MHz. The dielectric measurements were performed under different potentials (0 V, 0.5 V and 1 V) and amplitude of 10 mV. We determined the real (Z′) and imaginary (Z″) parts of the impedance of a system composed of two parallel stainless steel plates with dimensions of 64 × 21 mm and separated by a distance of 10 mm. The electrodes were cleaned in chloroform and subsequently immersed in deionized water in an ultrasonic bath. All experimental steps were performed at room temperature and repeated at least three times.

2.7. Scanning electron microscopy measurements

The scanning electron microscopy (SEM) images were obtained using a JSM 5900 (JEOL Instruments, Japan), at an acceleration voltage of 15 kV and a working distance of 5 μm. Samples were prepared on glass slides that were placed atop a SEM stub. After drying at room temperature, a thin gold layer was deposited atop by the use of a SCD 050 sputter coater (Bal-Tec, USA) [29].

2.8. Atomic force microscopy measurements

Atomic force microscopy (AFM) measurements were performed with a commercial PicoSPM II microscope (Molecular Imaging, USA). Cantilevers with a silicon tip with a resonance frequency of 297 kHz (Nanosensors, Switzerland) were used for the non-contact mode AFM in air at room temperature (approximately 25 °C).

2.9. Molecular modeling of Pa-MAP

The three-dimensional model for *Pa*-MAP was constructed according to Migliolo and coworkers [30], by using the PDB structure 1jb5 as template. The theoretical three-dimensional peptide structure was constructed by Modeller v.9.8 [31], using the template. The final model was chosen as the best one as determined after an evaluation using both PROSA II [32], to analyze packing and solvent exposure characteristics, and PROCHECK, for additional analysis of the stereochemical quality. In addition, RMSD was calculated by examining the degree of overlap of Cα traces and backbones onto the template structure with the program 3DSS [33]. The peptide structures were visualized and analyzed on Delano Scientific's PYMOL http://pymol.sourceforge.net/ [34]. The grand average of hydropathicity (GRAVY) was calculated using the ProtParam software [35].

2.10. In silico Pa-MAP versus DPPC membrane interaction

All docking calculations were performed using AUTODOCK 4.2 program [36]. Docking simulation of *Pa*-MAP was performed toward DPPC (64 lipids) membrane and 3864 water molecules [37]. All water molecules were removed and hydrogen atoms were added using the Auto Dock Tool. Grid maps were calculated with 35 × 35 × 20 and 1.0 Å spacing centered on the membrane surface and allowing interaction with all exposed head group. A Lamarckian genetic algorithm was used as the search method to find the best peptide–membrane complex. Fifty docking runs were implemented, totalizing 335 possible models for *Pa*-MAP *versus* DPPC membranes, where the maximum of freedom to the side chains was unlocked. The 335 generated structures were organized in a Box Plot to identify the greatest amount of interactions with lowest free energy, and the analysis showed a tolerance of 4 Å, as recommended for blind docking [38]. The program PyMol [39] was used to characterize peptide–membrane interactions. The statistical analyses were done through the R package for statistical computing (http://www.r-project.org).

3. Results

3.1. Electrochemical analysis of lipid–peptide interaction

Nyquist diagrams were taken before and after the modification with the electrode layer of DPPC and the addition of peptides *Pa*-MAP and LL-37 at concentrations of 10 and 100 μg mL^{-1}, and at different potentials, and they can be seen in Fig. 1. The phospholipid bilayer addition resulted in an increase in the semicircle diameter with respect to the electrode surface (Fig. 1a). A high resistance to charge transfer is associated to a low ion permeability, which can be achieved whenever lipids are densely packed and well-ordered [18]. The ability of a specific peptide to induce the permeation/lysis of a lipid membrane can be quantified by the percentage of leakage induced by these peptides [40]. When the AMPs induce membrane leakage, the membrane lipid is released and diluted, which leads to an increase on the conductivity of the solution that is proportional to the percentage of leakage [41]. After exposure to peptides, the lipid membrane can be gradually lost to the adjacent aqueous solutions, resulting in an empty space vacated by the loss of the membrane liquid. This behavior leads to the refill of this space by the aqueous solutions, a fact that is evidenced by the increase in the total capacitance and conductance [42]. With the addition of *Pa*-MAP, there was a sharp decrease (of approximately one order of magnitude) in resistance due to the lipid layer destabilization caused by the presence of the peptide. The difference found in the response between the two concentrations at diverse potentials of *Pa*-MAP shows that the peptide activity can be correlated to its concentration, with the maximum destabilization of the lipid membrane being observed when 100 μg mL^{-1} of peptide is present.

According to Chang et al.[18], the activity of AMPs depends on the type of lipids that constitutes the target membrane. We note that the partitioning, orientation and the degree of penetration of the peptides within the membranes [43] are extremely dependent on the values of

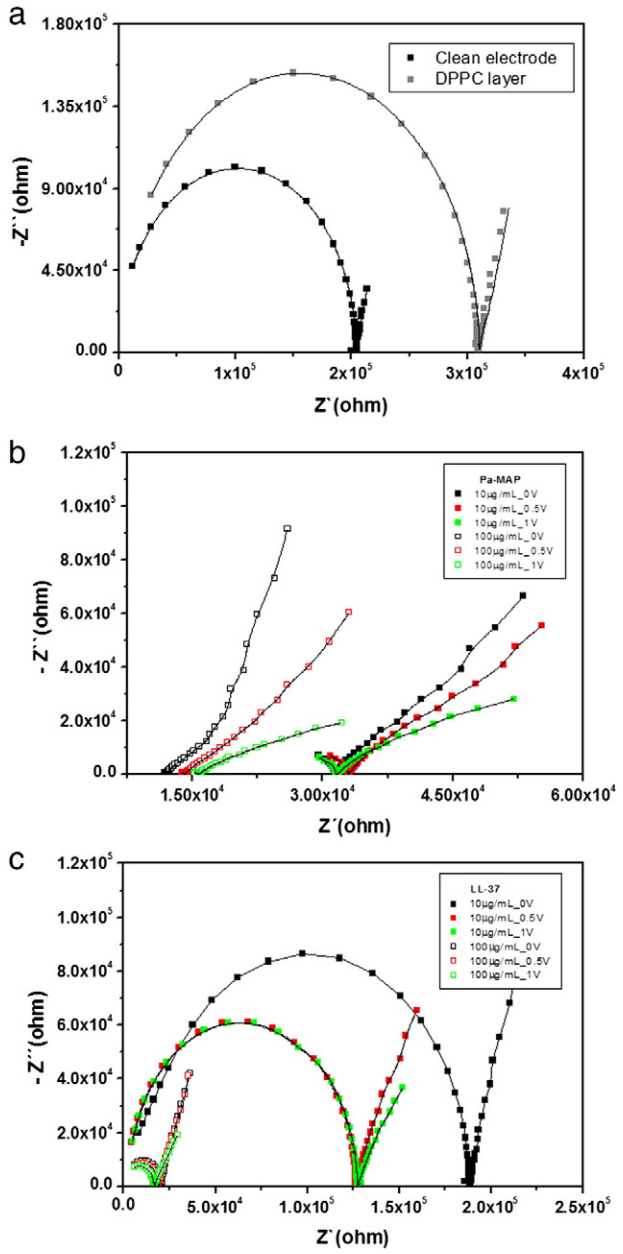

Fig. 1. Nyquist diagrams after different modification steps: clean electrode and after deposition of the membrane of DPPC (a), lipid layer after the addition of peptides *Pa*-MAP (b) and LL-37 (c) at different concentrations and potentials. Solid lines correspond to the fitting using the obtained circuit parameters.

the membrane potentials [44]. Also, the charge density of the membrane surface is affected by the bias potential due to the ion accumulation [18]. The *Pa*-MAP dielectric response was also influenced by the applied potential, although this effect was not very significant, with a higher response associated to the more positive potential (Fig. 1b). It is worth to note that it is possible to observe a different behavior in the Nyquist spectra for *Pa*-MAP, as compared to the other analyzed systems. The responses obtained are attributed to a different distribution of relaxation times due to the heterogeneities present at the microscopic level at the electrode/solution interface. In addition, this may result from the contributions from the static disorder due to porosity, as well as from the nonideal capacitive response of the interface [45]. In the case of the *Pa*-MAP system, we obtained a deformed impedance diagram as a result from the dislocation of the solution resistance due to the inhomogeneity or roughness of the electrode surface [46]. LL-37 showed a lower response compared to *Pa*-MAP, for all analyzed concentrations. However, the LL-37 activity had a clear correlation with an increase in concentration, with a decrease by about one order of magnitude being observed in the semicircle for the concentration of 100 µg mL^{-1}. Regarding the potential, LL-37 showed the highest response to more positive potentials, a fact that is most apparent at a concentration of 10 µg mL^{-1} (Fig. 1c). EIS is an useful technique to evaluate peptide–membrane interactions, since it allows either a controlled variation or to maintain the membrane potential during their interactions [18].

The impedance data were fitted by using the program EquivCRT [47]. The equivalent circuit obtained (Fig. 2) represents all elements of the biosystem analyzed in this study, as follows: the solution resistance (R_s), the resistance of the membrane to the passage of electric current (R_m) and of the electrode (R_e), the double layer capacitance of the membrane (C_m) and of the electrode (C_e), as well as the constant phase element (CPE). The first three elements are related to the kinetics of molecules and due to the ion flow and mass diffusion in the interface, while the latter three cases are related to the molecular or ionic polarization occurring in the interface. Recently, Zhu et al. [48] demonstrate the use of an equivalent circuit for complexes systems composed by 1,2-diphytanoyl-sn-glycero-3-phosphocholine and gramicidin. According to them, the ideal capacitances are replaced by the CPE, by considering the frequency dispersion of the capacitance as due to factors such as the inhomogeneity of the surface. The CPE response can be written as $Y_{CPE}(\omega) = Y_0(i\omega)^n$, where $0 < n < 1$. A CPE type of response, which reflects the non-homogeneity of the layer, is controlled by the parameter n (membrane homogeneity): CPE can be regarded as a pure capacitance when n is close to 1, and as a pure resistance, when n is close to 0 [49]. The changes in R_m are much higher than in other parts of the dielectric response, since this parameter depends on the characteristic resistance of insulation at the electrode/solution interface. Thus, the R_m was chosen as the relevant signal from the sensor. The corresponding circuit is commonly used in the literature, since it usually allows for a good fitting of the EIS experimental data.

In Fig. 3 we show real-time measurements of the curve R_m *vs.* time of action of *Pa*-MAP and LL-37. The addition of both peptides at different concentrations resulted in a drastic decrease in the membrane resistance within the first minute of exposure, that then remains constant until the end of the time of permanency (50 min). It is important to note that a large variation in the impedimetric response is not observed in the pristine membrane resistance under different applied potentials.

A summary of the results obtained before and after exposure of *Pa*-MAP and LL-37 is given in Table 1. All measurements were repeated at least three times and the results were the same nearly every time. These data demonstrate the efficiency of both peptides in membrane destabilization. At 0 V potential, the values of R_m in the presence of *Pa*-MAP dropped from 7.37×10^5 Ω to 4.14×10^4 Ω, at a concentration of 10 µg mL^{-1}, and to 4.40×10^3 Ω, at a concentration of 100 µg mL^{-1}. Otherwise, in the presence of LL-37 the values decreased to 1.91×10^5 Ω, at a concentration of 10 µg mL^{-1}, and 1.96×10^4 Ω, at a concentration of 100 µg mL^{-1}. Thus, a more efficient action in disrupting membranes was observed for *Pa*-MAP, as well as a dependence of action as a function of the concentration adopted for both peptides.

In relation to membrane homogeneity (n), the *Pa*-MAP and LL-37 activities induce a decrease in the n values (Table 1). However, it can be seen that after this reduction the n values remain constant after exposure to *Pa*-MAP. After exposure to the LL-37, in turn, there is a slight variation, indicating a greater membrane heterogeneity in behavior during exposure to this peptide (Table 1).

The analysis of *Pa*-MAP and LL-37 activities was also evaluated by varying the relative R_m (ΔR_m), which was calculated from the following equation:

$$\Delta R_m(\%) = \frac{R_m - R_m(pep)}{R_m} \times 100 \quad (1)$$

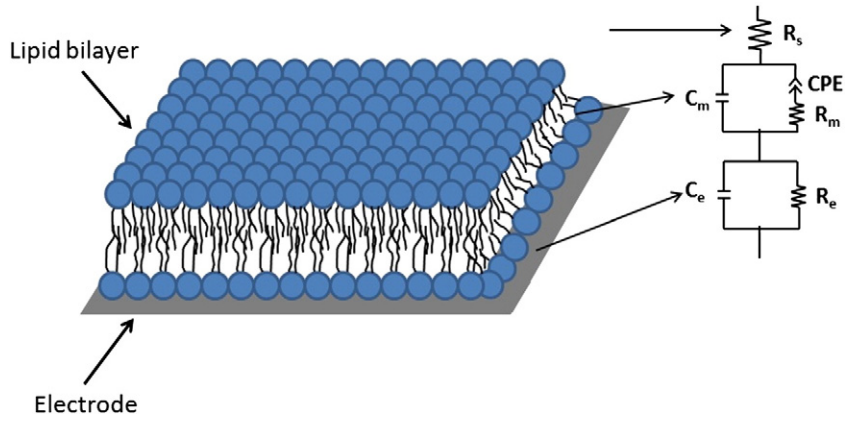

Fig. 2. A schematic representation of the electrode modified by a lipid layer (left) and its equivalent circuit (right). The elements R_s and C_m correspond to the solution resistance and double layer capacitance membrane, respectively. The elements in series R_mCPE correspond to the membrane resistance and the constant phase element, and the elements in parallel C_e, R_e correspond to the electrode double layer capacitance and resistance.

where R_m is the value of the resistance to the passage of electric current to the electrode modified by the membrane, and R_m (pep) is the resistance value of the passage of the electric current in the electrode modified by the membrane after exposure to peptides (*Pa*-MAP or LL-37).

As previously noted, the ΔR_m values were higher for *Pa*-MAP (around 94% for concentration 10 μg mL^{-1} and 99% for 100 μg mL^{-1}) than for LL-37 (approximately 75% concentration for 10 μg mL^{-1} and 97% for 100 μg mL^{-1}) (Table 1).

In the corresponding Bode plot it is possible to visualize that the presence of either *Pa*-MAP or LL-37 alters the electrical lipid membrane characteristics (Fig. 4). Especially for *Pa*-MAP, these differences are greater at higher concentrations. However, varying the intensity of the applied potential did not lead to significant differences in behavior. In the medium-frequency region, a linear relationship can be observed between the impedance modulus and the logarithm of the frequency (Fig. 4). This frequency region corresponds to the capacitive behavior of the electrode/solution interface.

In addition, as one can easily note, these two plots (Fig. 4b and c) show differences in the magnitude of the impedance at high frequency ranges when compared with those of the lipid-modified electrode; namely, the impedance magnitude of *Pa-MAP* and *LL-37* at high frequency was lower than in the absence of peptides (Fig. 4a). In addition, while there is a clear distinction between the dielectric responses of the peptide films of different concentrations, only small changes can be noticed in the impedance values at intermediate frequencies (Fig. 4). The decrease in the dielectric response for the peptide film (Fig. 4b and c) can be explained by an increase in the degree of displacement of ions near the surface.

3.2. Scanning electron microscopy (SEM)

In Fig. 5 we show SEM images of the membrane surface before and after exposure to *Pa*-MAP and LL-37. The clean electrode metal surface shows the presence of some defects (Fig. 5a). The layer of lipids appears

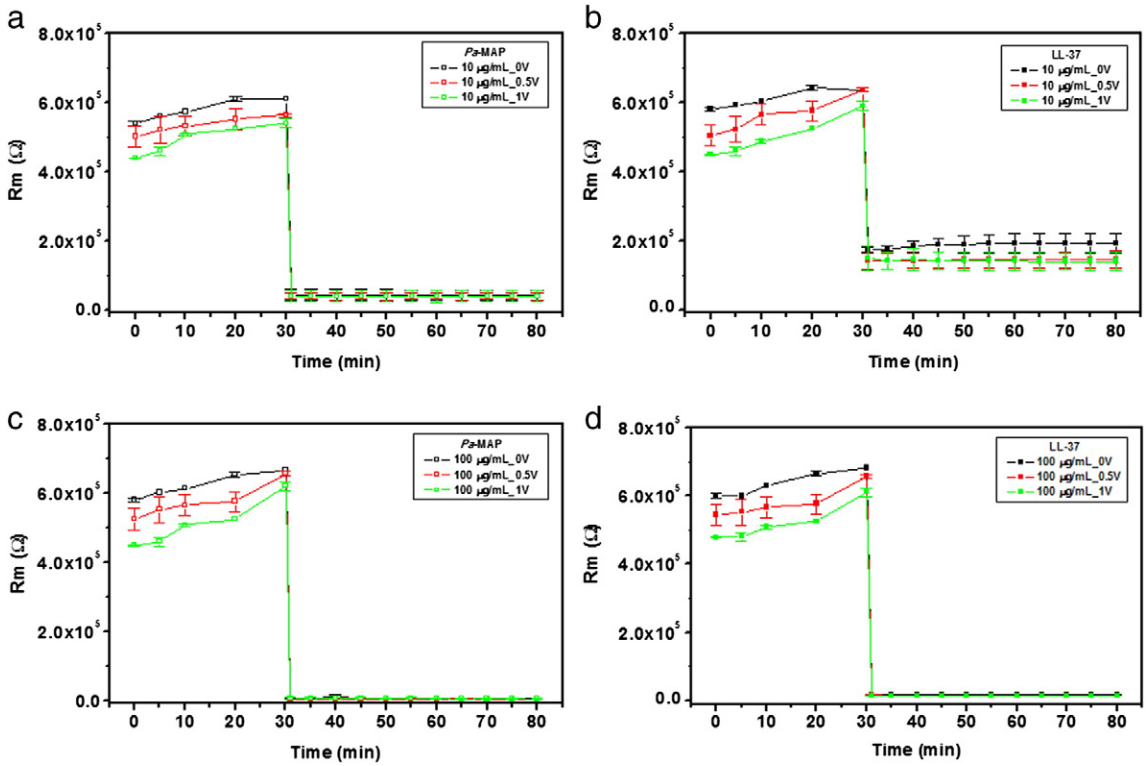

Fig. 3. Membrane resistance *versus* time at different potentials. In (a, b) the concentration used was 10 μg mL^{-1} and (c, d), 100 μg mL^{-1}. *Pa*-MAP and LL-37 were added in the 30th minute.

Table 1
Values of the equivalent circuit elements from fitted impedance results.

Sample	Peptide concentration (μg mL^{-1})	Exposure time (min)	R_m (Ω) $\times 10^4$	C_m (F) $\times 10^{-11}$	n	ΔR_m (%)
Lipid bilayer	–		73.70 ± 2.32	1.31 ± 0.50	–	–
Pa-MAP	10	1	4.27 ± 0.78	1.32 ± 0.40	0.78 ± 0.11	94.21 ± 2.55
Pa-MAP	10	25	4.19 ± 0.54	1.31 ± 0.51	0.78 ± 0.07	94.31 ± 1.50
Pa-MAP	10	50	4.14 ± 0.44	1.27 ± 0.37	0.78 ± 0.03	94.38 ± 2.40
Pa-MAP	100	1	0.31 ± 0.13	13.62 ± 1.13	0.81 ± 0.17	99.58 ± 3.18
Pa-MAP	100	25	0.35 ± 0.22	10.61 ± 1.26	0.81 ± 0.21	99.53 ± 2.21
Pa-MAP	100	50	0.44 ± 0.18	9.13 ± 1.09	0.81 ± 0.19	99.40 ± 3.31
LL-37	10	1	17.40 ± 1.12	1.01 ± 0.55	0.79 ± 0.10	76.39 ± 2.51
LL-37	10	25	19.11 ± 1.32	1.05 ± 0.19	0.78 ± 0.11	74.08 ± 3.29
LL-37	10	50	19.10 ± 1.25	1.05 ± 0.31	0.76 ± 0.08	74.08 ± 3.20
LL-37	100	1	1.91 ± 0.22	1.15 ± 0.44	0.77 ± 0.08	97.41 ± 3.33
LL-37	100	25	1.95 ± 0.19	1.16 ± 0.10	0.78 ± 0.10	97.35 ± 4.09
LL-37	100	50	1.96 ± 0.20	1.16 ± 0.73	0.78 ± 0.08	97.39 ± 3.43

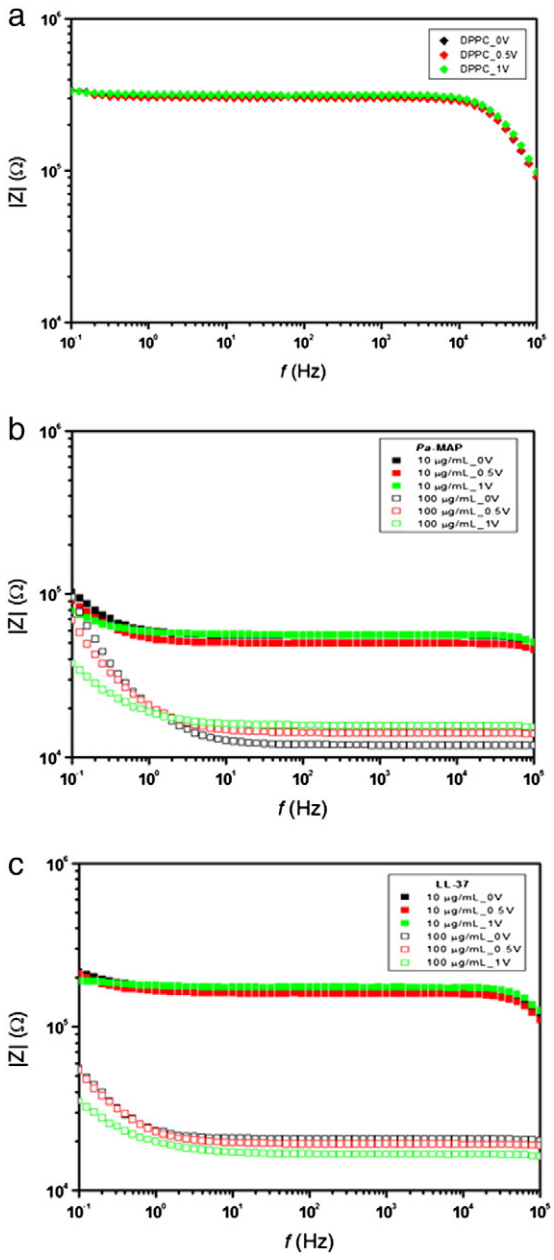

Fig. 4. Bode plot of the lipid membrane-modified electrode before (a) and after addition of *Pa*-MAP (b) and LL-37 (c) at different concentrations and potentials.

as a homogeneous and flat smooth surface atop the electrode (Fig. 5b). After exposure to *Pa*-MAP and LL-37, the lipid membrane became quite heterogeneous, forming a "carpet" with some flaws (Fig. 5c and 5d). It is important to note that the SEM images of *Pa*-MAP and LL-37 reveal a disruption of the membrane that can influence the conductivity of the solution, as well as the impedimetric responses of the systems (Fig. 1).

3.3. Atomic force microscopy (AFM)

The morphological differences of DPPC layers before and after the action of *Pa*-MAP and LL-37 can also be seen in AFM images obtained in non-contact mode (Fig. 6). Initially, the lipid bilayer that contains no peptide was defect-free and with typical round contour and a flat lamellar region. Through the topographic image was observed that the height of the phospholipid layer is around ~5 nm, in accord to previous studies for determination of lipid bilayer thickness [50,51] (Fig. 6a). Generally, the thickness of supported lipid bilayers can be determined by measuring the step height from the substrate to the top of the bilayer in bilayer defect regions [51].

Analysis of the lipid layers after the action of the studied peptides showed disruption of the layers, with formation of lipid domains of varying sizes, some larger with small holes and other of minor size. It is worth to note that the observed defects span the entire depth of the bilayer, suggesting that these structures are forming pores in the bilayer. In the case of LL-37, evaluating the morphology of the lipid membrane after the peptide interaction, it is possible to observe larger and heterogeneous surface lipid modifications compatible with previous results obtained by other authors [45] for the carpet mechanism. Similar results were obtained for *Pa*-MAP, with perturbations of the lipid membranes consisting of holes corresponding to a carpet or aggregate channel mechanisms [45,52]; detergent-like disruptions in the lipid membrane were also observed. The topographic image after the action of *Pa*-MAP and LL37 showed that the layers had an average thickness of about 8 nm (Fig. 6b and c).

In addition, the determination of the action mode of peptide in a lipid bilayer is difficult both for the experimental and theoretical models, since a single peptide may exhibit more than one action mode with the lipid bilayer, while the mechanism is concentration-dependent [48].

3.4. Evaluation in silico of lipid–peptide interaction

The peptide was left close to the DPPC membrane, allowing random contact with all surfaces since *Pa*-MAP demonstrated affinity for the DPPC membrane in *in vitro* assays, as previously reported [30]. The average value of the free energy observed for *Pa*-MAP toward the DPPC membrane was of (−3.1 ± 1.0) kcal mol^{-1} as demonstrated in a Box plot (Fig. 7a).

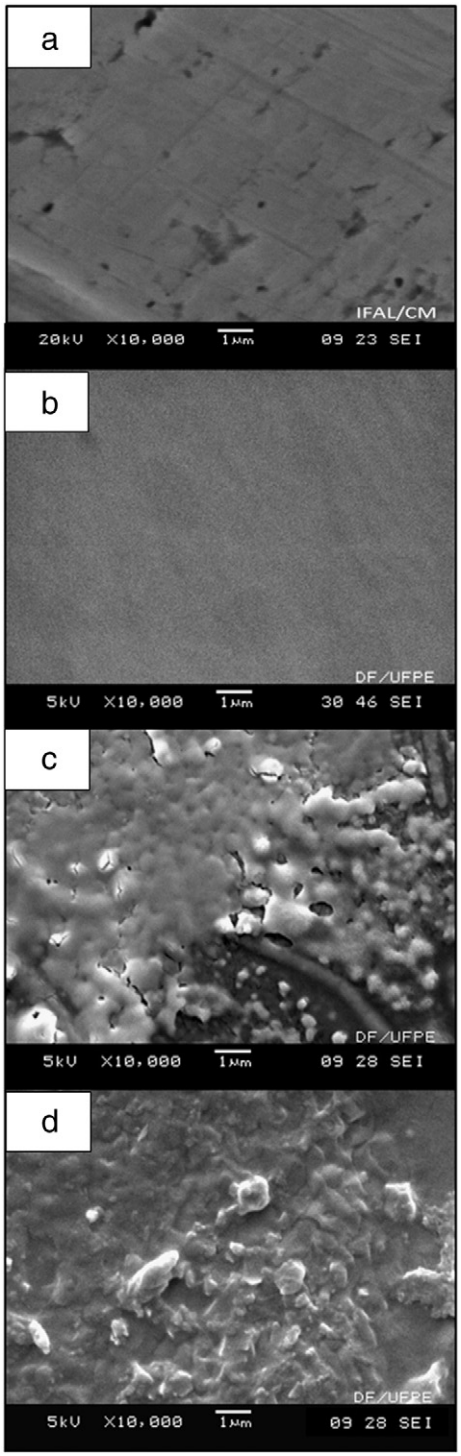

Fig. 5. SEM images of stainless steel substrate (a), layer DPPC before (b) and after exposure of *Pa*-MAP (c) and LL-37 (d).

The docking interaction analysis showed that *Pa*-MAP, which has high hydrophobicity (73%), appeared to be involved in interaction with the phospholipid carbons that compose the DPPC membrane (Fig. 7b and c). His^{1} interacts with $DPPC^{26}$ through of O13 and O14 (oxygen head group) with distances of 3.38 and 2.87 Å (table inside Fig. 7c). In addition, it was also possible to detect two hydrophobic interactions between His^{1} carbon of the imidazole ring (CD2 and CE1) attacking DPPC carbon (C3) with distances of 3.21 and 3.40 Å, respectively. Important interactions were also observed to occur between the Leu^{12} side chain carbon (CD1) and the $DPPC^{24}$ carbon (C14) at a distance of 2.74 Å, and a hydrogen bond between the amino acid Asn^{14} nitrogen (ND2) and the $DPPC^{14}$ oxygen head group (O13) at a distance of 3.40 Å. Furthermore, a hydrophobic link involving Ala^{14} carbon (CB) with $DPPC^{24}$ carbon (C14) was also observed on the membrane surface.

4. Discussion

Currently, several studies have been conducted in order to understand how the interaction of antimicrobial peptides with biomembranes takes place and to decipher the possible modes of action [18,19]. Several different mechanisms have been proposed to describe the AMPs' modes of action. Among these, four classical models are more relevant: barrel-stave, toroidal-pore, carpet and detergent [6]. According to the model barrel-stave, PAMs bind to the surface of the bilayer through electrostatic interaction and, on reaching a certain concentration at the membrane surface, the peptide monomers aggregate and become inserted in a perpendicular orientation into the hydrophobic core of the membrane. The toroidal-pore model is very similar to the barrel; however, in this model amphipathic peptide is incorporated according to their amphipathicity degree within the membrane, forming a pore linear peptide and lipid. In the fitted model, the AMPs are adsorbed on the membrane surface in parallel, forming an aggregate that covers the surface of the lipid bilayer as a "carpet" of molecules. Upon reaching critical concentration, the membrane is destroyed/solubilized. Finally, the model detergent is based on intercalation of AMPs in lipid bilayers and, when reaching a critical micelle concentration (CMC), forming micellar structures in a manner similar to a detergent [53,54]. For this reason, some authors have described this effect as a detergent model extension carpet, after the concentration of peptides on the membrane reaching a high value [16,54]. In fact, the study of action mechanism of AMPs to permeate phospholipid membranes is essential to the understanding of their antibiotic function.

In practice, it does not seem possible to distinguish between these models, although all the mechanisms mentioned above have two common steps. The first is the electrostatic interaction between the cationic peptides and the anionic lipids present in microbial membranes, and this is followed by a second step. which consists of a peptide reorganization over the phospholipid bilayer that leads to pore formation and, consequently, to a permeability increase, which suggests the occurrence of membrane destruction [55].

EIS has been used in studies of peptide/membrane interaction, since this technique monitors the lipid membrane integrity in real time and is sensitive to membrane property modifications, such as thickness, uniformity and ion permeability. It has been successfully used in different studies to understand the AMPs' mechanisms of action [15,18].

Faradaic impedance spectra obtained by EIS follow a behavior pattern that includes a semicircular portion observed at higher frequencies, corresponding to the transferring electron process in the electrode-solution interface, followed by a linear lower frequency part assigned to mass transport limited by diffusion [56]. The increased resistance observed in the Nyquist diagram after adding the phospholipid molecules is a characteristic that can be associated with resistance load transfer, since addition of phospholipids on the electrode hinders the passage of electrons, increasing the resistance of the system. The technique for forming self-organized BLMs on solid substrates is based on different driving forces between the metallic surface and the amphiphilic lipid molecules [57–59], which occur between a highly hydrophillic solid surface interacting and the polar groups of the lipid molecules [60]. Also, the interaction and orientation between the phospholipid and the metal surface could be explained by metal–polymer interface theory [58] based on the interaction between the metal and oxygen atoms. The interaction of phospholipid polar headgroups with a metal surface is similar to a specific adsorption and the strength of this bond between oxygen atoms of the phosphate group of the phospholipids and the solid

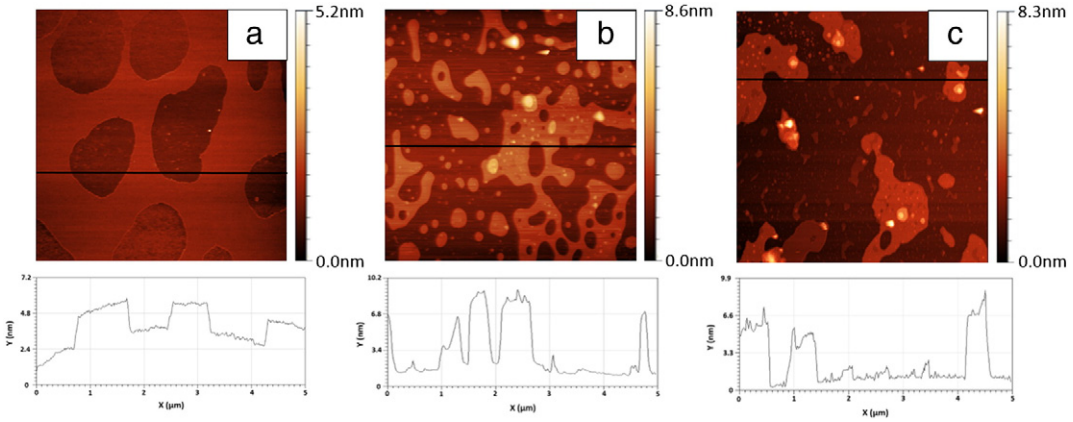

Fig. 6. AFM topographic image obtained for layer DPPC before (a) and after exposure to *Pa*-MAP (b) and LL-37 (c) with the corresponding cross section. Scan area was 5 μm × 5 μm.

surface is dependent on the chemical reactivity of the metal [23]. Thus, the chemical reactivity between the lipid and the metal surface explains the observed stability over time of the measurements performed EIS. In addition, the interaction of phospholipid molecules and the metal surface is favored by the presence of irregularities on the metal surface [58].

The sudden fall of resistance after addition of the *Pa*-MAP and LL-37 may be explained by the destabilization of the membrane caused by the peptides, thus allowing the passage of electrons on the electrode surface. Regarding the influence of applied potential on the response of the peptides, as it was observed in this study, other studies have shown that the movement of ions from the interface of the monolayer can be influenced by external potentials. Boubour and Lennox [61] studied the ionic permeability in the self-assembled monolayers using impedance spectroscopy under different potentials in the absence of redox active species. Defects caused by the applied potentials have been found in the lipid membranes. During cathodic potentials, the energy required for migration of ions through the membrane decreases, facilitating the transfer of electrons [61]. Therefore, such behavior can explain the responses obtained at more positive potentials for the peptides investigated, since at positive potentials the membrane shows low resistance to charge transfer.

The activity of AMPs is basically associated to charge and hydrophobicity properties. These two physicochemical characteristics, which are related to the selectivity of the peptides to membranes, facilitate the interaction with fatty acyl chains [6]. The AMs selectivity for microbial membranes and the absence of deleterious effects on membranes of mammals are important points to be highlighted in the use of these peptides in the pharmaceutical area. In general, AMPs are cationic and have high affinity for negatively charged lipids (a major component of bacterial membranes) [17].

The results obtained from adjustments using the program EquivCRT demonstrate how efficient are *Pa*-MAP and LL-37 in destabilizing membranes. For both peptides, the Rm fell sharply in the first minute of exposure. LL-37 is a 37-amino acid peptide (LLGDFFRKSKEKIGKEFKRIVQRIKDFLRNLVPRTES-NH_2), 16 of which are charged at physiological pH (11 positive and 5 negative, resulting in a net charge of +6) [25]. This peptide was shown to bind to and permeate effectively within both zwitterionic and negatively charged

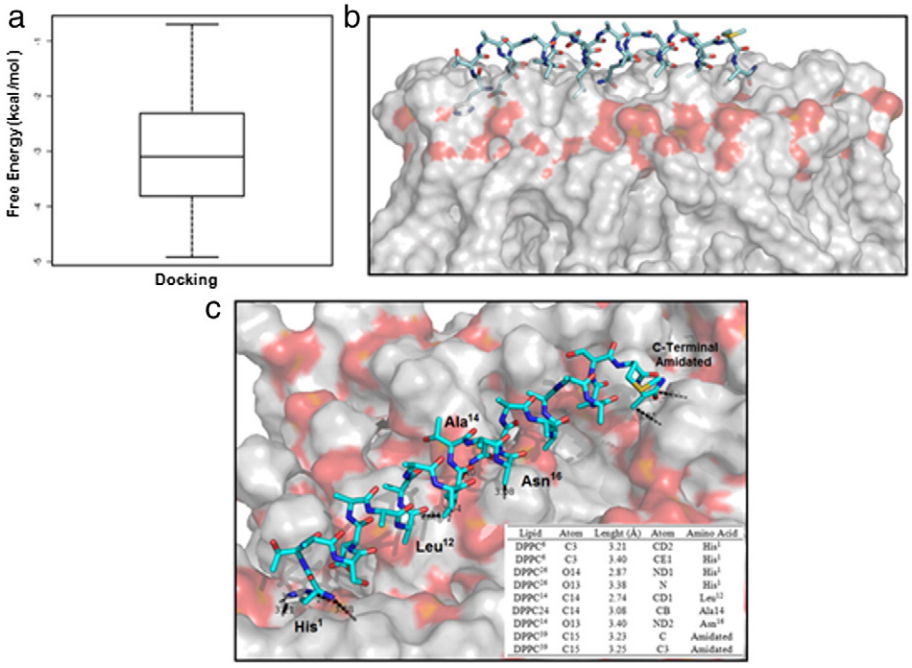

Fig. 7. *Pa*-MAP *in silico* docking analysis with DPPC membrane. (a) Box plot of 335 interaction models ranked according to the free energy. (b) Side visualization of *Pa*-MAP forward DPPC membrane showing the peptide insertion and (c) zoom visualization showing peptide interaction, with detailed interaction being showed in the inner table with lipid and amino acid position and their respective atom names and interaction length.

phospholipids, a feature that distinguishes LL-37 from most other antimicrobial peptides, which act selectively on bacterial cells. This affinity for zwitterionic membranes also suggests the occurrence of hydrophobic interactions between the peptides and the membranes [62]. Otherwise, the poly-alanine *Pa*-MAP (HTASDAAAAAALTAANAAAAAAASMA-NH_2) displays a lower net charge (−1) and, accordingly, a slight anionic pI (5.08). Moreover, the hydrophobicity was also distinct in the two peptides. LL37 shows as a hydrophobic ratio of 35% and a Boman index of 2.99 kcal mol^{-1}. Otherwise, the *Pa*-MAP hydrophobic ratio is much higher, reaching to 73% with a lower −0.23 kcal mol^{-1}. Initially named protein-binding potential by Hans Boman, this index was renamed as Boman Index after introduced into the Antimicrobial Peptide Database (http://aps.unmc.edu/AP/main.php). In summary, Boman index is the sum of the free energies of side chains for transfer from cyclohexane to water divided by the total number of the AMP amino acid residues [63]. The Boman index assesses the potential for a protein or peptide to interact with other proteins. A high Boman index value suggests that an AMP may play a wide variety of different roles within the cell, due to its ability to interact with multiple proteins.

It is worth noting that, despite being neutrally charged, *Pa*-MAP showed higher activity against Gram-negative bacteria, as compared to Gram-positive bacteria [30]. As previously discussed, cationic residues may in most cases play an important role in the first step, due to electrostatic interaction. The importance of cationic residues has been proven in the last few years. Mutations of arginine and lysine residues can modify the total activity of AMPs, such as mellitin (a peptide from *Apis mellifera*), resulting in a greater toxicity to mammalian cells [64]. However, this feature does not seem to be a determinant in the affinity of the *Pa*-MAP by membrane, since the corresponding hydrophobicity ratio seems to play an essential role in the second step, pore forming [62]. The absence of these cationic residues in *Pa*-MAP shows that its activity is driven by hydrophobic interactions and this also explains its lack of toxicity to mammalian cells [30]. Therefore, this behavior may contribute to the higher response obtained for *Pa*-MAP as compared to LL-37, since this peptide has a higher hydrophobic ratio (73%) [30].

The activity of the peptides on the membranes also appears to influence the membrane homogeneity (n). The fall in homogeneity should be attributed to disruptions caused by the presence of peptides. However, the constancy of the values of n after *Pa*-MAP action indicates that membranes exposed to this peptide tend to show more effective lipid reorganization than membranes exposed to LL-37.

The AMP activities here evaluated may affect both the capacitance and the resistance of the membranes. For an ideal membrane, no ion is transported across the bilayer (which presents infinite resistance), while the membrane behaves like a dielectric medium with charges accumulating on both sides. A finite membrane resistance determines the ion diffusion rate through the bilayer [18]. Therefore, the membrane instability caused by the interaction with the peptides results in an increased C_m and a decrease in R_m, as one can see in Table 1.

Chang et al. [18] conducted a study with two AMPs, where it was possible to distinguish the modifications in the parameters based on peptide modes of action (resistance, capacitance and homogeneity of membrane), as perceived by EIS. If the peptides act by following a barrel-stave model, the resistance of the membrane drops and the thickness and homogeneity of the membrane are unaltered, as observed for melittin [18]. Otherwise, if the peptides act as prescribed by the toroidal pore model, the membrane also becomes permeable (R_m decreases) and the membrane thickness in the pore regions decreases, resulting in a slight decrease in its homogeneity. According to this model, the toroidal pores act as gates for the peptides' passage across the membrane. Thus, the pore formation may be transient, disintegrating over time as the concentration of the peptides on both sides of the membrane becomes balanced. This leads to an increase in membrane resistance as observed for magainin [18].

For peptides that act following the carpet model, the membrane homogeneity decreases, while the resistance can decrease (in the case of peptides that introduce a disorder in lipids) or increased (if the peptides cause an ordering of lipids). It is worth noting that peptides that act according to this model can induce a detergent effect. These peptides in high concentrations can disrupt the membrane, resulting in a huge reduction (or even complete disappearance) of the membrane resistance. However, the membrane can still provide an electrochemical barrier, where affected regions are repaired by redistributing lipids and/or peptides by lateral diffusion from the intact regions. Thus, the uniformity decreases due to the existence of intact and repaired disrupted regions [18]. This model is consistent with the observed data for the peptides here described, confirming the work described above [62], which indicated the carpet model as a mechanism of action for LL-37, and suggesting this same mechanism for *Pa*-MAP. The presence of both peptides caused a destabilization of the membrane in the first minutes of exposure; subsequently, these changes are locally repaired, providing a measurable resistance.

The evaluation of *in silico Pa*-MAP–DPPC interaction allowed the results obtained for electrochemical analysis to be complemented, in addition to improving the understanding of the possible mechanism of action of *Pa*-MAP. In previous similar studies for two cyclic peptides, named amp-1 and amp-2, acting toward Gram-negative and -positive membranes, the corresponding output energy was reported as −6.4 and −5.8 kcal mol^{-1} and −5.7 and −7.5 kcal mol^{-1}, respectively [65]. The *in silico* data here obtained (−3.1 kcal mol^{-1}) suggested that *Pa*-MAP presents a lower affinity for DPPC when compared with the free energy observed for amp-1 and amp-2. The *in silico* data corroborated the *in vitro* data [30], indicating that *Pa*-MAP has activity (MIC 30 μM) in higher concentration due to the absence of charged amino acid residues. As an example to be compared, the pleurocidin from *P. americanus* and pardaxin isolated from *Pardachirus marmoratus* [66] presented MIC values of 3.5 and 3.0 μM, respectively.

The docking interaction analysis showed that the interaction between *Pa*-MAP and membrane involved a mix of electrostatic and mainly hydrophobic interaction guided by Leu^{12} and Ala^{16} amino acid residues. His^{1}, Asn^{16} and amidated C-termini are *Pa*-MAP amino acid residues that may be involved with anchorage in membrane. The interaction might first be guided through hydrogen bonds. After that, the presence of *Pa*-MAP at higher concentrations could lead to pore formation, due to the presence of hydrophobic amino acid residues that could bind to membrane by van der Waals forces.

These data corroborate the impedance data obtained (Figs. 3 and 4), in which some time is necessary to cause membrane interaction, besides explaining the formation of a "carpet" as observed in Fig. 5.

4. Conclusions

Our results demonstrated that the peptide *Pa*-MAP has the potential to destabilize membranes, an observation that may explain the *in vitro* antimicrobial activity observed [30]. The responses obtained through EIS for LL-37 successfully demonstrated that this peptide followed a carpet model mode of action. In addition, the dominance of this model was also determined by other authors using diverse techniques [62, 67]. For *Pa*-MAP, the data suggest that the mechanism of action of *Pa*-MAP is also that of a patterned carpet, but with a detergent effect appearing in the range of concentrations used in this study. The mechanism of action of *Pa*-MAP was first described here. Finally, the potential-independent activity of *Pa*-MAP suggests that the peptide can act on a wide range of pathogenic microorganisms (membranes with anionic, cationic and zwitterionic molecules), in agreement with previous *in vitro* results.

Acknowledgements

The authors are grateful for the support from the Rede de Nanobiotecnologia/CAPES, INCT_IF (Instituto Nacional de Ciência e Tecnologia para Inovação Farmacêutica), CNPq (grant 310305/2012-8

and 310361/2012-5), FAPDF and FACEPE. J.M. Nascimento would like to thank CAPES for a PhD scholarship. Moreover, the authors are also grateful for the technical assistance of Prof. Etelino F. de Melo from the Instituto Federal Tecnológico de Alagoas for SEM measurements.

References

[1] S.M. Mandal, S. Dey, M. Mandal, S. Sarkar, S. Maria-Neto, O.L. Franco, Identification and structural insights of three novel antimicrobial peptides isolated from green coconut water, Peptides 30 (2009) 633–637.
[2] E. Strandberg, P. Tremouilhac, P. Wadhwani, A.S. Ulrich, Synergistic transmembrane insertion of the heterodimeric PGLa/magainin 2 complex studied by solid-state NMR, Biochim. Biophys. Acta 1788 (2009) 1667–1679.
[3] R.E. Hancock, H.G. Sahl, Antimicrobial and host-defense peptides as new anti-infective therapeutic strategies, Nat. Biotechnol. 24 (2006) 1551–1557.
[4] L.J. Zhang, A. Rozek, R.E.W. Hancock, Interaction of cationic antimicrobial peptides with model membranes, J. Biol. Chem. 276 (2001) 35714–35722.
[5] L.T. Nguyen, E.F. Haney, H.J. Vogel, The expanding scope of antimicrobial peptide structures and their modes of action, Trends Biotechnol. 29 (2011) 464–472.
[6] K. Lohner, The role of membrane lipid composition in cell targeting of antimicrobial peptides, in: K. Lohner (Ed.), Development of Novel Antimicrobial Agents: Emerging StrategiesHorizon Scientific Press, 2001, pp. 149–165.
[7] M.J. Kuiper, J.V. Fecondo, M.G. Wong, Rational design of alpha-helical antifreeze peptides, J. Pept. Res. 59 (2002) 1–8.
[8] Z. Gong, K.V. Ewart, Z. Hu, G.L. Fletcher, C.L. Hew, Skin antifreeze protein genes of the winter flounder, *Pleuronectes americanus*, encode distinct and active polypeptides without the secretory signal and prosequences, J. Biol. Chem. 271 (1996) 4106–4112.
[9] L.D. Teixeira, O.N. Silva, L. Migliolo, I.C.M. Fensterseifer, O.L. Franco, In vivo antimicrobial evaluation of an alanine-rich peptide derived from *Pleuronectes americanus*, Peptides 42 (2013) 144–148.
[10] N. Papo, Y. Shai, Can we predict biological activity of antimicrobial peptides from their interactions with model phospholipid membranes? Peptides 24 (2003) 1693–1703.
[11] R. Jelinek, S. Kolusheva, Membrane interactions of host-defense peptides studied in model systems, Curr. Protein Pept. Sci. 6 (2005) 103–114.
[12] T. Martynski, H.T. Tien, Spontaneous assembly of bilayer-membranes on a solid-surface, Bioelectrochem. Bioenerg. 25 (1991) 317–324.
[13] H.T. Tien, A.L. Ottova, Supported planar lipid bilayers (s-BLM) as electrochemical biosensors, Electrochim. Acta 43 (1998) 3587–3610.
[14] H.T. Tien, R.H. Barish, L.Q. Gu, A.L. Ottova, Supported bilayer lipid membranes as ion and molecular probes, Anal. Sci. 14 (1998) 3–18.
[15] J. Lin, J. Motylinski, A.J. Krauson, W.C. Wimley, P.C. Searson, K. Hristova, Interactions of membrane active peptides with planar supported bilayers: an impedance spectroscopy study, Langmuir 28 (2012) 6088–6096.
[16] A.S. Ladokhin, S.H. White, 'Detergent-like' permeabilization of anionic lipid vesicles by melittin, Biochim. Biophys. Acta 1514 (2001) 253–260.
[17] M.D.L. Oliveira, O.L. Franco, J.M. Nascimento, C.P. de Melo, C.A.S. Andrade, Mechanistic aspects of peptide–membrane interactions determined by optical, dielectric and piezoelectric techniques: an overview, Curr. Protein Pept. Sci. 14 (2013) 543–555.
[18] W.K. Chang, W.C. Wimley, P.C. Searson, K. Hristova, M. Merzlyakov, Characterization of antimicrobial peptide activity by electrochemical impedance spectroscopy, Biochim. Biophys. Acta 1778 (2008) 2430–2436.
[19] J.M. Nascimento, O.L. Franco, M.D.L. Oliveira, C.A.S. Andrade, Evaluation of magainin I interactions with lipid membranes: an optical and electrochemical study, Chem. Phys. Lipids 165 (2012) 537–544.
[20] H.T. Tien, Z. Salamon, Formation of self-assembled lipid bilayers on solid substrates, Bioelectrochem. Bioenerg. 22 (1989) 211–218.
[21] H.P. Yuan, A. Leitmannova-Ottova, H.T. Tien, An agarose-stabilized BLM: a new method for forming bilayer lipid membranes, Mater. Sci. Eng. C 4 (1996) 35–38.
[22] V.I. Pasechnik, S.A. Ivanov, T. Hianik, M. Shnejdarkova, B. Sivak, Conductivity fluctuations in bilayer lipid membranes, formed on the support, Biofizika 43 (1998) 61–68.
[23] M. Snejdarkova, M. Rehak, M. Otto, Stability of bilayer lipid membranes on different metallic supports, Biosens. Bioelectron. 12 (1997) 145–153.
[24] F. Neville, M. Cahuzac, O. Konovalov, Y. Ishitsuka, K.Y. Lee, I. Kuzmenko, G.M. Kale, D. Gidalevitz, Lipid headgroup discrimination by antimicrobial peptide LL-37: insight into mechanism of action, Biophys. J. 90 (2006) 1275–1287.
[25] E. Sevcsik, G. Pabst, A. Jilek, K. Lohner, How lipids influence the mode of action of membrane-active peptides, Biochim. Biophys. Acta Biomembr. 1768 (2007) 2586–2595.
[26] E. Borenfreund, J.A. Puerner, Toxicity determined in vitro by morphological alterations and neutral red absorption, Toxicol. Lett. 24 (1985) 119–124.
[27] J. Murphy, M. Kies, Note on the spectrophotometric determination of proteins in dilute solutions, Biochim. Biophys. Acta 3 (1960) 382–384.
[28] D. Ivnitski, E. Wilkins, H.T. Tien, A. Ottova, Electrochemical biosensor based on supported planar lipid bilayers for fast detection of pathogenic bacteria, Electrochem. Commun. 2 (2000) 457–460.
[29] H.P. de Oliveira, C.A.S. Andrade, C.P. de Melo, Electrical impedance spectroscopy investigation of surfactant–magnetite–polypyrrole particles, J. Colloid Interface Sci. 319 (2008) 441–449.
[30] L. Migliolo, O.N. Silva, P.A. Silva, M.P. Costa, C.R. Costa, D.O. Nolasco, J.A.R.G. Barbosa, M.R.R. Silva, M.P. Bemquerer, L.M.P. Lima, M.T.V. Romanos, S.M. Freitas, B.S. Magalhães, O.L. Franco, Structural and functional characterization of a multifunctional alanine-rich peptide analogue from *Pleuronectes americanus*, Plos one 7 (2012) e47047.
[31] N. Eswar, B. Webb, M.A. Marti-Renom, M.S. Madhusudhan, D. Eramian, M.Y. Shen, U. Pieper, A. Sali, Comparative protein structure modeling using Modeller, Curr. Protoc. Bioinforma. 2 (2007).
[32] M. Wiederstein, M.J. Sippl, ProSA-web: interactive web service for the recognition of errors in three-dimensional structures of proteins, Nucleic Acids Res. 35 (2007) W407–W410.
[33] K. Sumathi, P. Ananthalakshmi, M.N. Roshan, K. Sekar, 3dSS: 3D structural superposition, Nucleic Acids Res. 34 (2006) W128–W132.
[34] W. DeLano, The PyMOL molecular graphics system, 2002.
[35] T.J. Dolinsky, J.E. Nielsen, J.A. McCammon, N.A. Baker, PDB2PQR: an automated pipeline for the setup of Poisson–Boltzmann electrostatics calculations, Nucleic Acids Res. 32 (2004) W665–W667.
[36] G.M. Morris, R. Huey, W. Lindstrom, M.F. Sanner, R.K. Belew, D.S. Goodsell, A.J. Olson, Autodock4 and AutoDockTools4: automated docking with selective receptor flexiblity, J. Comput. Chem. 16 (2009) 2785–2791.
[37] S.J. Marrink, O. Berger, D.P. Tieleman, F. Jaehnig, Adhesion forces of lipids in a phospholipid membrane studied by molecular dynamics simulations, Biophys. J. 74 (1998) 931–943.
[38] J. Jitonnom, K. Lomthaisong, V.S. Lee, Computational design of peptide inhibitor based on modifications of proregion from *Plutella xylostella* midgut trypsin, Chem. Biol. Drug Des. 79 (2012) 583–593.
[39] W.L. DeLano, The PyMOL Molecular Graphics System, Version 1.3r1, Schrodinger, LLC, New York, 2010.
[40] E.E. Ambroggio, F. Separovic, J.H. Bowie, G.D. Fidelio, L.A. Bagatolli, Direct visualization of membrane leakage induced by the antibiotic peptides: maculatin, citropin, and aurein, Biophys. J. 89 (2005) 1874–1881.
[41] M.M. Domingues, M.A.R.B. Castanho, N.C. Santos, rBPI(21) promotes lipopolysaccharide aggregation and exerts its antimicrobial effects by (hemi)fusion of PG-containing membranes, Plos One 4 (2009).
[42] F.F. Zha, H.G.L. Coster, A.G. Fane, A study of stability of supported liquid membranes by impedance spectroscopy, J. Membr. Sci. 93 (1994) 255–271.
[43] M.S. Sansom, Alamethicin and related peptaibols — model ion channels, Eur. Biophys. J. 22 (1993) 105–124.
[44] S. Stankowski, U.D. Schwarz, G. Schwarz, Voltage-dependent pore activity of the peptide alamethicin correlated with incorporation in the membrane: salt and cholesterol effects, Biochim. Biophys. Acta 941 (1988) 11–18.
[45] F. Contu, B. Elsener, H. Bohni, Characterization of implant materials in fetal bovine serum and sodium sulfate by electrochemical impedance spectroscopy. I. Mechanically polished samples, J. Biomed. Mater. Res. 62 (2002) 412–421.
[46] A.P.F. Turner, I. Karube, G.S. Wilson, Biosensors — Fundamentals and Applications, Oxford Science Publications, 1989.
[47] B.A. Boukamp, A package for impedance/admittance data analysis, Solid State Ionics 18 (1986) 136–140.
[48] Z.-W. Zhu, Y. Wang, X. Zhang, C.-F. Sun, M.-G. Li, J.-W. Yan, B.-W. Mao, Electrochemical impedance spectroscopy and atomic force microscopic studies of electrical and mechanical properties of nano-black lipid membranes and size dependence, Langmuir 28 (2012) 14739–14746.
[49] Z. Kerner, T. Pajkossy, Impedance of rough capacitive electrodes: the role of surface disorder, J. Electroanal. Chem. 448 (1998) 139–142.
[50] S.J. Johnson, T.M. Bayerl, D.C. Mcdermott, G.W. Adam, A.R. Rennie, R.K. Thomas, E. Sackmann, Structure of an adsorbed dimyristoylphosphatidylcholine bilayer measured with specular reflection of neutrons, Biophys. J. 59 (1991) 289–294.
[51] A. Mecke, D.K. Lee, A. Ramamoorthy, B.G. Orr, M.M.B. Holl, Membrane thinning due to antimicrobial peptide binding: an atomic force microscopy study of MSI-78 in lipid bilayers, Biophys. J. 89 (2005) 4043–4050.
[52] R. Bals, X.R. Wang, M. Zasloff, J.M. Wilson, The peptide antibiotic LL-37/hCAP-18 is expressed in epithelia of the human lung where it has broad antimicrobial activity at the airway surface, Proc. Natl. Acad. Sci. U. S. A. 95 (1998) 9541–9546.
[53] K. Hall, H. Mozsolits, M.I. Aguilar, Surface plasmon resonance analysis of antimicrobial peptide–membrane interactions: affinity & mechanism of action, Lett. Pept. Sci. 10 (2003) 475–485.
[54] K.A. Brogden, Antimicrobial peptides: pore formers or metabolic inhibitors in bacteria? Nat. Rev. Microbiol. 3 (2005) 238–250.
[55] H. Sato, J.B. Feix, Peptide–membrane interactions and mechanisms of membrane destruction by amphipathic alpha-helical antimicrobial peptides, Biochim. Biophys. Acta 1758 (2006) 1245–1256.
[56] J.R. Macdonald, Impedance spectroscopy, Ann. Biomed. Eng. 20 (1992) 289–305.
[57] K. Miyano, Interfaces as a field for arranging organic-molecules, Jpn. J. Appl. Phys. Part 1 (24) (1985) 1379–1388.
[58] H. Leidheiser, P.D. Deck, Chemistry of the metal–polymer interfacial region, Science 241 (1988) 1176–1181.
[59] H.T. Tien, Z. Salamon, J. Kutnik, P. Krysinski, J. Kotowski, D. Ledermann, T. Janas, Bilayer lipid-membranes (Blm) — an experimental system for biomolecular electronic device development, J. Mol. Electron. 4 (1988) S1–S30.
[60] Z. Salamon, Y. Wang, G. Tollin, H.A. Macleod, Assembly and molecular-organization of self-assembled lipid bilayers on solid substrates monitored by surface-plasmon resonance spectroscopy, Biochim. Biophys. Acta Biomembr. 1195 (1994) 267–275.
[61] E. Boubour, R.B. Lennox, Potential-induced defects in n-alkanethiol self-assembled monolayers monitored by impedance spectroscopy, J. Phys. Chem. B 104 (2000) 9004–9010.
[62] Z. Oren, J.C. Lerman, G.H. Gudmundsson, B. Agerberth, Y. Shai, Structure and organization of the human antimicrobial peptide LL-37 in phospholipid membranes: relevance to the molecular basis for its non-cell selective activity, Biochem. J. 341 (1999) 501–513.
[63] H.G. Boman, Antibacterial peptides: basic facts and emerging concepts, J. Intern. Med. 254 (2003) 197–215.

[64] J.A. Werkmeister, A. Kirkpatrick, J.A. McKenzie, D.E. Rivett, The effect of sequence variations and structure on the cytolytic activity of melittin peptides, Biochim. Biophys. Acta 1157 (1993) 50–54.
[65] S.M. Mandal, L. Migliolo, O.L. Franco, The use of MALDI-TOF-MS and in silico studies for determination of antimicrobial peptides' affinity to bacterial cells, J. Am. Soc. Mass Spectrom. 23 (2012) 1939–1948.
[66] A.J. Mason, I.N.H. Chotimah, P. Bertani, B. Bechinger, A spectroscopic study of the membrane interaction of the antimicrobial peptide pleurocidin, Mol. Membr. Biol. 23 (2006) 185–194.
[67] K.A. Henzler-Wildman, G.V. Martinez, M.F. Brown, A. Ramamoorthy, Perturbation of the hydrophobic core of lipid bilayers by the human antimicrobial peptide LL-37, Biochemistry 43 (2004) 8459–8469.